Polymorph-Dependent Phosphorescence of Cyclometalated Platinum(II) Complexes and Its Relation to Non-covalent Interactions

Elina V. Sokolova, Mikhail A. Kinzhalov,* Andrey S. Smirnov, Anna M. Cheranyova, Daniil M. Ivanov, Vadim Yu. Kukushkin, and Nadezhda A. Bokach*

Read Online

ACCESS | Metrics & More | Article Recommendations | Supporting Information

ABSTRACT: Cyclometalated platinum(II) complexes $[Pt(ppy)Cl(CNAr)]$ (ppy = 2-phenylpyridinato-C^2,N; Ar = C_6H_4-2-I **1**, C_6H_4-4-I **2**, C_6H_3-2-F-4-I **3**, and C_6H_3-2,4-I_2 **4**) bearing ancillary isocyanide ligands were obtained by the bridge-splitting reaction between the dimer $[Pt(ppy)(\mu\text{-Cl})]_2$ and 2 equiv any one of the corresponding CNAr. Complex **2** was crystallized in two polymorphic forms, namely, $\mathbf{2^I}$ and $\mathbf{2^{II}}$, exhibiting green (emission quantum yield of 0.5%) and orange (emission quantum yield of 12%) phosphorescence, respectively. Structure-directing non-covalent contacts in these polymorphs were verified by a combination of experimental (X-ray diffraction) and theoretical methods (NCIplot analysis, combined electron localization function (ELF), and Bader quantum theory of atoms in molecules (QTAIM analysis)). A noticeable difference in the spectrum of non-covalent interactions of $\mathbf{2^I}$ and $\mathbf{2^{II}}$ is seen in the Pt···Pt interactions in $\mathbf{2^{II}}$ and absence of these metallophilic contacts in $\mathbf{2^I}$. The other solid luminophores, namely, **1**, $\mathbf{3^{I-II}}$, **4**, and **4**·$CHCl_3$, exhibit green luminescence; their structures include intermolecular C−I···Cl−Pt halogen bonds as the structure-directing interactions. Crystals of **1**, $\mathbf{2^I}$, $\mathbf{3^I}$, $\mathbf{3^{II}}$, **4**, and **4**·$CHCl_3$ demonstrated a reversible mechanochromic color change achieved by mechanical grinding (green to orange) and solvent adsorption (orange to green).
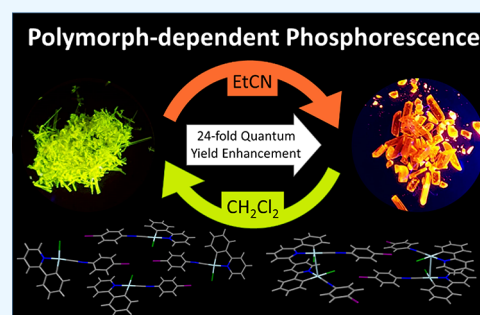
1. INTRODUCTION

Transition metal-based luminescent materials are a subject of rapidly growing interest in view of their applications for design and fabrication of solid-state lighting devices,[1−7] in chemo-sensing,[8−11] and as photocatalysts.[12−15] Efficient room temperature (RT) phosphorescence of transition-metal species is conventionally attributed to the heavy atom effect that induces strong spin−orbit coupling, which facilitates both fast intersystem crossing and the formally spin-forbidden triplet radiative decay.[16−18] The photophysical and photochemical properties of transition-metal species, particularly those of platinum(II), have been analyzed in a number of reviews.[16,17,19−23]

The luminescent properties of metal complex-based materials are closely associated with their molecular conformations and also with crystal packing determined in particular by intermolecular interactions;[24−26] thus, different polymorphs of the same compound could exhibit different photophysical properties. The control over the formation of polymorphs is challenging because of the complexity of multiple molecule−molecule and molecule−solvent interactions that occurred on crystallization. In contrast to octahedral d^6-Ru^{II} and d^6-Ir^{III} complexes, d^8-Pt^{II}-based species usually adopt a square-planar coordination geometry with open axial coordination sites facilitating non-covalent binding to Pt^{II}

centers. These non-covalent linkages can significantly alter both ground and excited-state properties of Pt^{II}-based systems and, hence, photophysical parameters.[20,27−31]

Thus, metallophilic interactions and intermolecular π-stacking strongly change the emission profile and shift the radiation to the red region, which can be explained by the change in the nature of the excited state from an MLCT to MMLCT.[32−36] At the same time, aggregation due to other contacts, for example, halogen bonding or d_z^2···π-hole interactions, as a rule does not lead to a change in the emission color but can be accompanied by an increase in the emission quantum yield (hereinafter abbreviated as EQY) of luminescence.[37−40]

Significant differences in the luminescence EQYs for polymorphs of platinum(II) complexes have been detected in only few cases.[29,41,42] In two out of three reports, a polymorph exhibiting short Pt···Pt contacts displayed 2-[42] and 12-fold[29]

greater-phosphorescence EQYs than those measured for the other polymorph—without Pt···Pt metallophilic interactions. In the third study, one out of three obtained polymorphs does not exhibit luminescence, while the other two emissive polymorphs exhibit a sixfold difference of their EQYs. The latter two polymorphs do not display Pt···Pt contacts[41] and, as indicated by the original authors, "different quantum yields may be ascribed to the different local packings of the independent molecules in the polymorphs."

In this study, the complexes [Pt(ppy)Cl(CNAr)] (ppy = 2-phenylpyridinato-C^2,N; Ar = C_6H_4-2-I **1**, C_6H_4-4-I **2**, C_6H_3-2-F-4-I **3**, and C_6H_3-2,4-I_2 **4**; Figure 1) were crystallized under
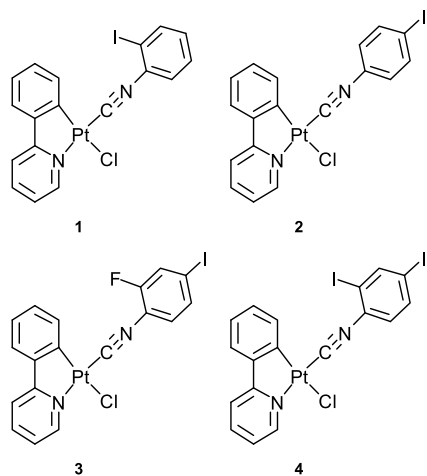

Figure 1. Molecular structures of platinum(II) complexes **1**−**4**.

different conditions. In the case of **2**, two polymorphic forms exhibiting a 24-fold difference in EQYs and also different emission profiles were obtained. We analyzed structure-directing non-covalent contacts by experimental and theoretical methods and hypothesized which intermolecular forces could lead to this polymorph-dependent phosphorescence. All our data are consequently detailed in the following sections.

2. RESULTS AND DISCUSSION

2.1. Synthesis and Crystal Growth. Cyclometalated platinum(II) complexes bearing ancillary isocyanide ligands are promising candidates for optoelectronic applications since they exhibit strong RT phosphorescence in combination with useful properties such as thermal and chemical stability (for recent reports, see refs 43−46). Cyclometalated species **1**−**4** were prepared and isolated in moderate to high yields (61−94%) by the bridge-splitting reaction between the dimer [Pt(ppy)(μ-Cl)]$_2$ and 2 equiv any one of the corresponding isocyanides: CNC_6H_3-2-X^1-4-X^2, X^1 = H, F, I; X^2 = H, I; reflux for 3 h in MeCN); the structures of **1**−**4** were confirmed by IR and ^{1}H, $^{13}C\{^1H\}$, and $^{195}Pt\{^1H\}$ NMR spectroscopy, mass spectrometry, and single-crystal X-ray diffractometry (XRD). For details, see Sections S3−S5.

Complexes **1**−**4** were crystallized under different conditions including solvent, temperature, and concentration variations (Experimental Section). In the case of **1**, only one type of crystal was obtained, while the crystallization of **2**−**4** gave two polymorphs (denoted as 2^{I-II} and 3^{I-II} for **2** and **3**, respectively) or a solvent-free form (**4**) and crystal solvate (**4**·CHCl$_3$) of high quality and homogeneity; all these species were characterized by XRD (Section 2.2). We observed that all

crystals (apart from orange polymorph 2^{II}) are yellow, which is typical for [Pt(ppy)Cl(CNR)]-type complexes.

2.2. Structure-Directing Non-covalent Interactions. Inspection of the XRD data combined with the Hirshfeld surface analysis[47] (for the Hirshfeld diagrams, see Section S6) revealed and visualized the structure-directing intermolecular non-covalent contacts such as C−I···Cl−Pt halogen bonding (abbreviated as HaB; found in all structures) and metallophilic Pt···Pt interactions (observed exclusively for polymorph 2^{II}). Since polymorphs 2^{I} and 2^{II} exhibit different photophysical properties (Figure 2, detailed in Section 2.3), we attempted to highlight their structural features and speculate how they might be related to the different luminescent properties of the polymorphs.
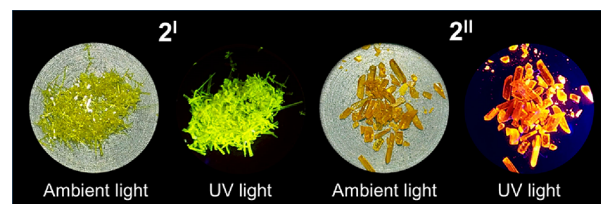

Figure 2. Images of 2^{I} and 2^{II} crystals under ambient and ultraviolet (365 nm, portable UV lamp) light.

The asymmetrical unit of 2^{I} contains four crystallographically independent molecules in two conformations (two 2^{I}-a and two 2^{I}-b; Figure 3), which differ from each other by the orientation of the isocyanide aryl relatively the Pt coordination plane. For 2^{I}-a, the isocyanide aryl group is almost coplanar with the Pt(C∩N, C, Cl) plane (4.1(2)° for 2^{I}-a1 and 11.42(18)° for 2^{I}-a2; Table S5.3), whereas in 2^{I}-b the angle between the coordination plane (C∩N, C, Cl) and the isocyanide aryl plane is much larger (55.29(17)° for 2^{I}-b1 and 67.29(18)° for 2^{I}-b2). The C−I···Cl−Pt HaBs (0.90−0.91 $\sum_{vdW}$, Bondi;[48] 0.87−0.88 $\sum_{vdW}$, Alvarez[49]) is formed by the interaction between the σ-(I)-hole of coplanar 2^{I}-a and a Cl atom of twisted 2^{I}-b. The Pt···I−C semicoordination bonds (1.01−1.03 $\sum_{vdW}$, Bondi;[48] 0.87−0.88 $\sum_{vdW}$, Alvarez[49]) are formed by the interaction between the Pt atom of coplanar 2^{I}-a and an electron belt of the I atom of another neighboring twisted 2^{I}-b. Simultaneously, the twisted 2^{I}-b is a face-to-face dimer that formally occurred by the symmetric C−I···I−C (0.89−0.91 $\sum_{vdW}$, Bondi;[48] 0.87−0.88 $\sum_{vdW}$, Alvarez[49]) interaction between two arene iodine centers, and these contacts are attributed to type I halogen−halogen contact[50,51] (Table S6.2). Accordingly, the pair of C−I···Cl−Pt HaBs and the symmetric C−I···I−C short contact link two coplanar 2^{I}-a and two twisted 2^{I}-b to a tetrameric supramolecular architecture.

In contrast to 2^{I}, the structure of 2^{II} contains only one type of crystallographically independent planar molecule (the dihedral angle is 6.39(11)°), which is arranged in the helical chain held by HaB (Figure 4). In 2^{II}, we observed short [3.2058(3) Å; 0.93 $\sum_{vdW}$, Bondi,[48] and 0.70 $\sum_{vdW}$, Alvarez[49]] Pt···Pt separations between planes of 2^{II} in the dimeric structure, which then forms the supramolecular double zigzag via the system of the HaB and Pt···Pt interactions.

The structures of **1**, 3^{I}, 3^{II}, **4**, and **4**·CHCl$_3$ contain one type of crystallographically independent complex, where an interplay between σ-(I)-hole and a chloride accomplishes a head-to-tail supramolecular dimer (3^{I}; Figure 5A), 1D supramolecular
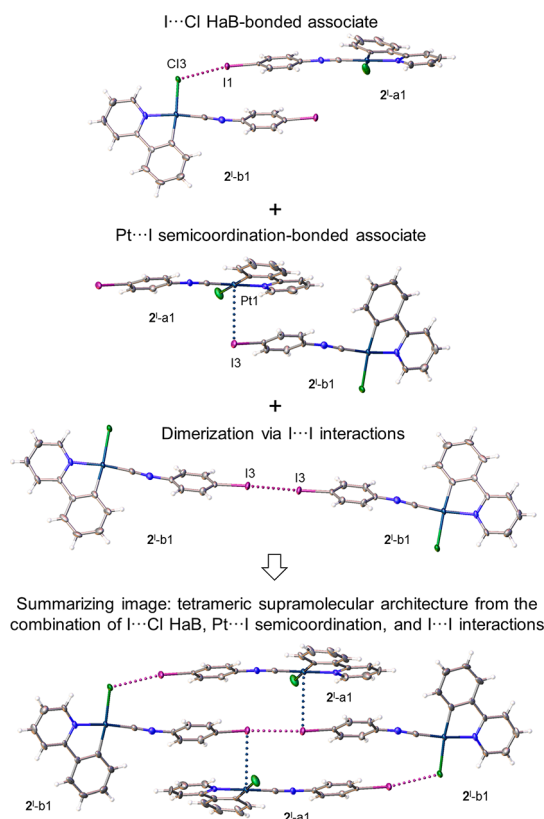
Figure 3. Tetrameric supramolecular architecture of 2^I that occurred by the interplay of the HaB (purple dots), Pt···I semicoordination (blue dots), and I···I (purple dots) interactions. Crystallographically independent molecules 2^I-a2 and 2^I-b2 are similar to 2^I-a1 and 2^I-b1, and views of their structures are given in the Supporting Information (Figure S6.8).
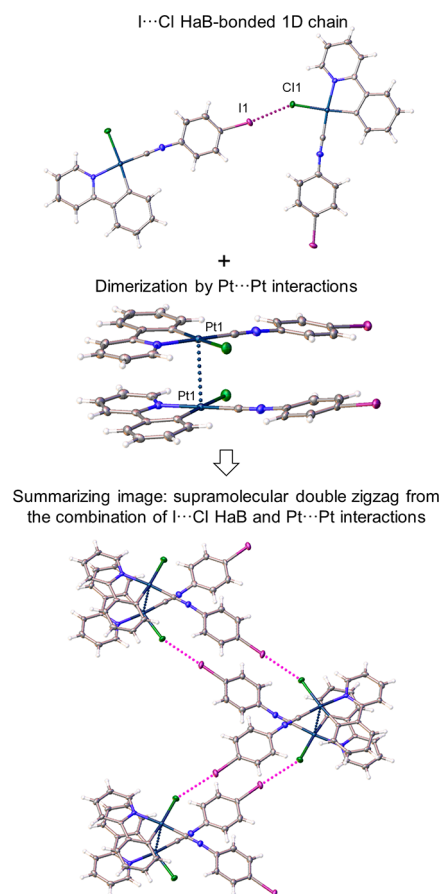

Figure 4. Supramolecular double zigzag of 2^{II} that occurred by the interplay of the HaB (purple dots) and Pt···Pt (blue dots) interactions.

polymers with a 1D zigzag arrangement (**1** and **4**; Figure 5B), or a helical chain held by HaB (**3^{II}** and **4·CHCl$_3$**; Figure 5C). These crystals display intermolecular Pt···Pt separations of >4.0 Å, which is significantly larger than the Bondi Pt + Pt van der Waals radii's sum (3.44 Å), and this comparison indicates the absence of any meaningful contacts between two Pt centers. The structural features of these species are detailed in Section S6. Thus, the absence of metallophilic interactions in the structures of **1**, **3^I**, **3^{II}**, **4**, and **4·CHCl$_3$** is their common feature, which is the same as that for the **2^I** polymorph.

2.3. Solid-State Luminescence Properties. *2.3.1. Solid-State Luminescence.* In general, all our solid species are emissive materials (Table S7.1 and Figure 6), but efficiency of luminescence is different, particularly for polymorphs **2^I** and **2^{II}**. Yellow crystals of **2^I** and all crystalline forms of the other species, namely, **1**, **3^I**, **3^{II}**, **4**, and **4·CHCl$_3$**, exhibit a green emission (λ_{max} of 509–522 nm; Figure 6) with very similar luminescence spectra profiles. The solid-state luminescence spectra of **1**, **2^I**, **3^I**, **3^{II}**, **4**, and **4·CHCl$_3$** are similar to those observed for **1–4** in CH$_2$Cl$_2$ solutions (the photophysical properties in solution are detailed in Section S7), thus providing evidence favoring the absence of any metal···metal short contacts in all these structures.

In contrast to green-emissive yellow polymorph **2^I** (λ_{max} of 522 nm; Φ_{em} of 0.5%), orange polymorph **2^{II}** displayed an unstructured band in the orange region (λ_{max} 586 nm) with a 24-fold higher EQY (Φ_{em} of 12%). This strong 24-fold increase of the EQY in **2^{II}** compared to **2^I** is probably associated with an

increase in structural rigidity upon the formation of a supramolecular double-zigzag due to the synergistic combination of HaB and Pt···Pt interactions (Figure 4). Note that, in this context, a few previous reports[29,30] indicated an efficiency of solid-state luminescence for those polymorphs that exhibit Pt···Pt interactions, and EQY enhancement was attributed to "inhibition of the thermal dispersion of photoenergy from the excited state"[42] or by "inhibition of vibrational quenching by the formation of the rigid dimer".[29]

2.3.2. Mechanochromic Behavior. Some phosphorescent Pt^{II} complexes could also display mechanochromic luminescence behavior (for relevant reviews, see refs 52 and 53). The luminescent mechanochromism was observed for all yellow crystals (namely, **1**, **2^I**, **3^I**, **3^{II}**, **4**, and **4·CHCl$_3$**), but it was not detected for orange crystals of **2^{II}**. Grinding of these yellow crystals results in their color change from yellow to orange; the color change is reversed on treatment with a solution or even vapors of CH$_2$Cl$_2$. Irradiation of the finely ground orange **1**, **2^I**, **3^I**, **3^{II}**, **4**, and **4·CHCl$_3$** with 365 nm UV light leads to orange luminescence (564–601 nm; Figure S7.3 and Table S7.2), which is close to the emission profile of orange crystals of **2^{II}** (λ_{max} of 586 nm). In contrast to **2^I**, grinding of orange crystals **2^{II}** in an agate mortar does not lead to any visible changes in the photoluminescence; ground powders of **2^{II}** display an identical emission with that of ground powder of **2^I**. In all cases, grinding led to a decrease in the luminescence emission quantum yields (Table S7.2).
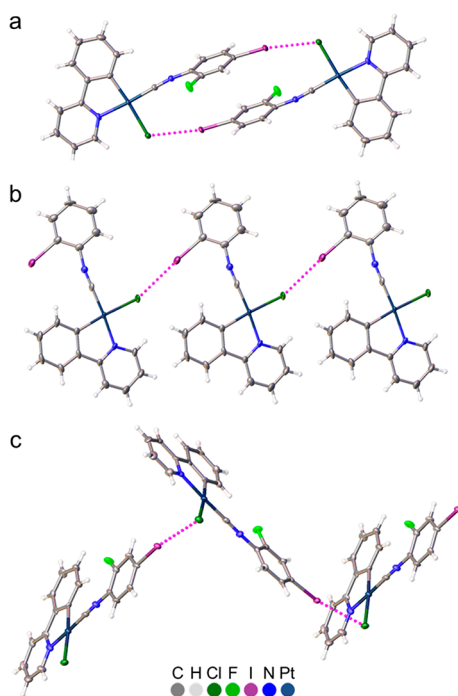
Figure 5. Fragments of the representative crystal structures showing a head-to-tail supramolecular dimer (3^I, a), 1D supramolecular polymers with a 1D zigzag (**1**, b), and a helical (3^{II}, c) chain. The HaB are given by dotted lines. Structures **4** (zigzag chain) and **4·**CHCl$_3$ (helical chain) are similar, and they are given in Figures S6.7 and S6.11.

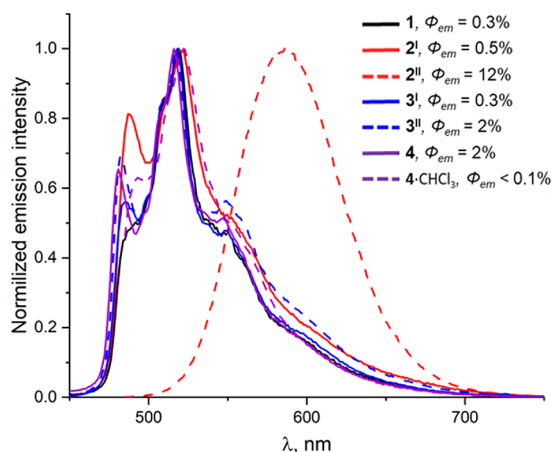**Figure 6.** Normalized solid-state emission spectra for **1**−**4** (298 K).

The powder X-ray diffraction (PXRD) studies of finely ground 2^I and 2^{II} show only low-intensity diffraction peaks from the starting crystals, indicating the amorphization upon grinding (Figures S5.8 and S5.9). We assumed accordingly that the mechanochromism of 2^I is based on crystalline-to-amorphous phase transitions. On grinding, the color and luminescence of 2^{II} was not changed, although the PXRD data indicate the change from a crystalline state to an amorphous phase (Figure S5.9). The mechanical grinding-triggered luminescence switches of some solid platinum(II) complexes have previously been reported.[46,54−59] In all these studies, a structure-less emissive band and red shift of the emissive maxima after grinding were assigned to the occurrence of emissive aggregates packed in close proximity through Pt···Pt

and/or $\pi \cdots \pi$ interactions. The mechanochromic luminescence of ground samples of **1**, 2^I, 3^I, 3^{II}, **4**, and **4·**CHCl$_3$ exhibiting orange luminescence can be reversed either by addition to the ground powders of a few drops of CH$_2$Cl$_2$ or by exposure to dichloromethane vapor; the reversible mechanochromic behavior, illustrated in Figure 7, is similar to that observed recently for the [Pt(ppy)Cl(CNC$_6$H$_4$-2,6-Me$_2$)] complex.[46]
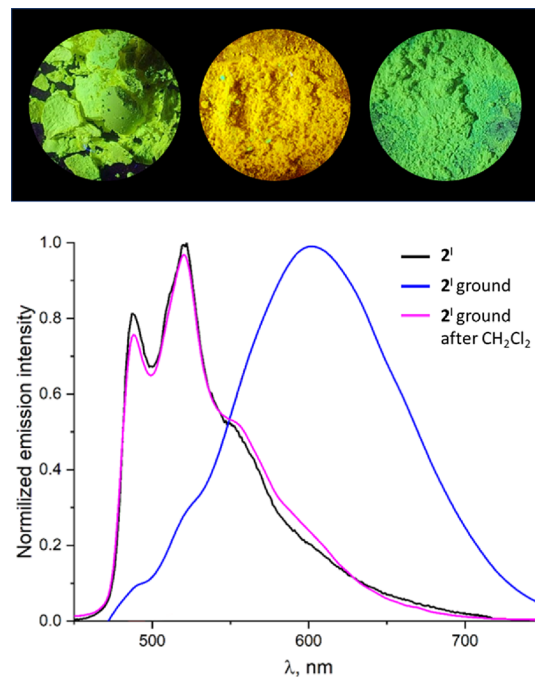

Figure 7. Top: reversible mechanochromism of 2^I before grinding (left), after grinding (center), and after addition of a drop of CH$_2$Cl$_2$ to the ground sample (right). The images were obtained under 365 nm UV irradiation. Bottom: normalized emission spectra of 2^I before grinding, after grinding, and after addition of a drop of CH$_2$Cl$_2$ to the ground sample.

Thus, we demonstrated that six (**1**, 2^I, 3^I, 3^{II}, **4**, and **4·**CHCl$_3$) out of seven studied structures exhibited similar green emission under 365 nm UV irradiation at RT, while only 2^{II} is an orange emitter. The longer wavelength and the non-structured emission of 2^{II} are consistent with low-lying spin-forbidden triplet metal−metal-to-ligand-charge transfer (^{3}MMLCT) transitions;[60] these transitions are in agreement with the identified Pt···Pt short contact.

2.4. Theoretical Studies of Non-covalent Interactions.
It is undoubtedly attractive to associate the solid-state phosphorescence with the presence of a certain type (or certain system) of non-covalent interaction(s). However, by having only one example of differing photophysical properties of polymorphs, it is hardly possible to reveal the underlying factors of such distinct behavior. To reveal these factors, an extensive set of statistical data is needed, which, we hope, will be gradually accumulated in the literature.

At this stage, one can only examine the existing structure-determining interactions to simplify the analysis of polymorph-dependent phosphorescence for future relevant studies. Therefore, we left aside the puzzle of multiple hydrogen bonds—the fraction of which is significant in almost all organometallic systems—and focused on the study of halogen bonding and metallophilic interactions in the two polymorphs

of **2**. The Hirshfeld surface analysis (Section S6) indicates that these interactions, in addition to the hydrogen bond, greatly contribute to the stabilization of both crystal structures. An additional factor, which stimulated our interest in studying these types of intermolecular interactions, is based on the previous reports that verified the strong effect of HaB[37−39] and metallophilic interactions[33,35] on the photophysical characteristics of platinum(II) complexes (see the Introduction).

Several approaches, such as analysis of the molecular electrostatic potential (MEP),[61−63] NCIplot[64,65] analysis, combined electron localization function (ELF),[66−68] and Bader's quantum theory of atoms in molecules (QTAIM analysis),[69] were applied to reveal structure-determining non-covalent interactions in the two phosphorescent polymorphs.

2.4.1. MEP Analysis. The MEP surfaces of all our structures were computed in order to study the most electron-poor and electron-rich regions of this molecules (Figure 8 and Figures
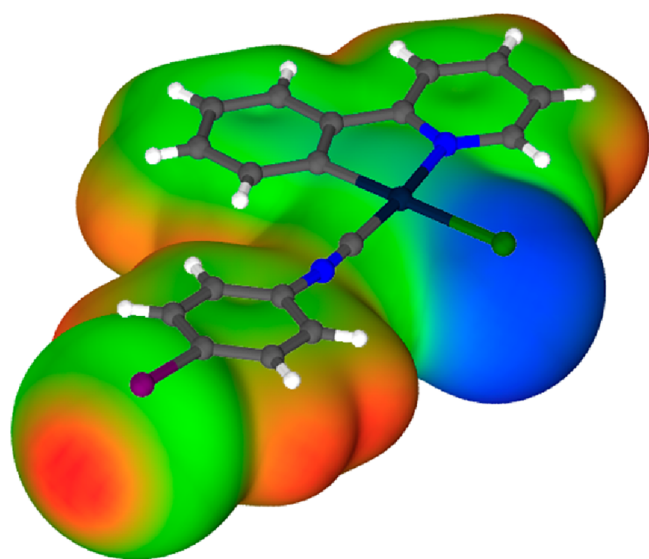

Figure 8. MEP surface of **2**[II]. Isosurface of 0.001 au. The energies at selected points are given in kcal/mol. The color scheme is from Politzer et al.[70,71] MEP surfaces of all other discussed molecules are given in Figure S8.2.

S8.1 and S8.2). An analysis of the MEP surfaces reveals that the MEP maximum is located at the σ-hole of the I-substituent of arene from isocyanides (HaB donors), ranging from +27.6 to +32.6 kcal/mol. Notably, the value of the σ-hole in different conformers, that is, coplanar **2**[I]-a1 (+27.7 kcal/mol) and twisted **2**[I]-b2 (+27.6 kcal/mol) are slightly different, which indicates the little effect of conformation on the value of the σ-hole. The MEP minimum is located at the coordinated chloride in compounds **1**−**4**, ranging from −41.9 to −39.5 kcal/mol. This result strongly agrees with the occurrence of HaBs in the solid state.

2.4.2. Combined QTAIM and NCIplot Analysis. We evaluated energetically the non-covalent interactions using DFT calculations and also characterized them by a combination of QTAIM and NCIplot analyses (Figure 9 and Figures S8.3−S8.12). In all model clusters, the non-covalent interactions are characterized by the (3, −1) bond critical points (BCPs) and bond paths connecting the atoms. The QTAIM parameters at the bond CPs are gathered in Tables S8.1−S8.4.
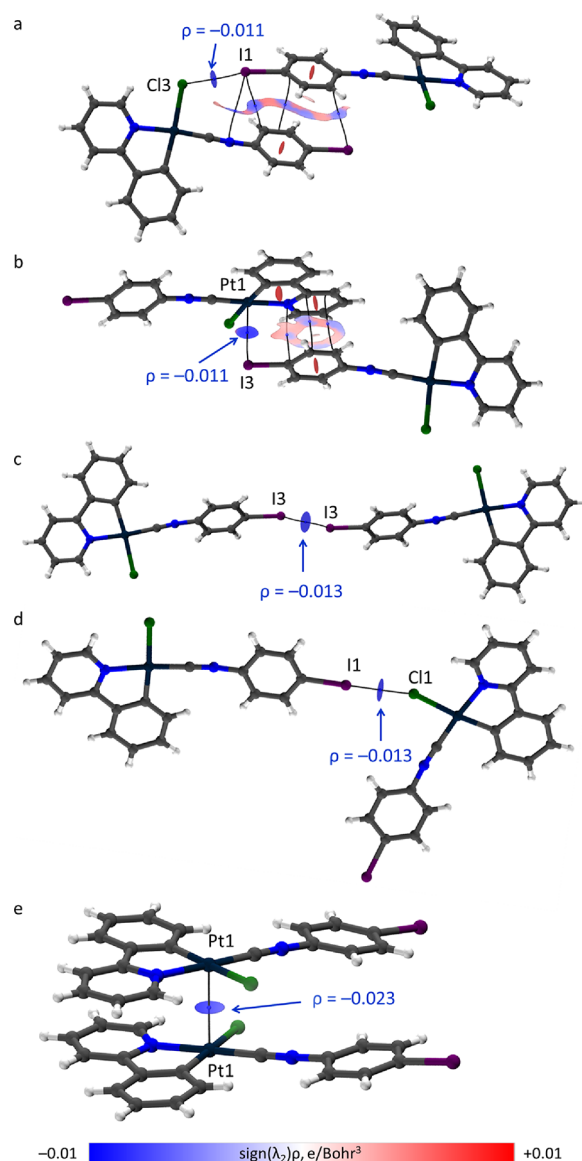

Figure 9. QTAIM distribution of bond CP (blue spheres) and bond paths for the cluster (**2**[I]-a−**2**[I]-b) (a) and (**2**[II])$_2$ (d) formed by I···Cl HaBs, the cluster (**2**[I]-a−**2**[I]-b) formed by Pt···I semicoordination (b), the cluster (**2**[I]-b)$_2$ formed by I···I interactions (c), and (**2**[II])$_2$ formed by Pt···Pt interactions (e). The NCIplot index isosurfaces are also represented using a 0.3−0.4 (e$^{1/3}$ bohr)$^{−1}$ isovalue. The color range is −0.01 e/bohr^3 ≤ sign(λ_2)ρ ≤ 0.01 e/bohr^3. Only CPs and NCIplot surfaces characterizing intermolecular interactions in a−d are represented for clarity; for e, only the CP and NCIplot surface characterizing Pt···Pt interactions are given in detailed diagram, which includes all interactions between the molecules, as shown in Figure S8.7.

2.4.3. Analysis of ELF and ED/ESP Minima. The philicities of non-covalently interacting partners can be determined by ELF projections with critical points and bond paths from a QTAIM electron density topology, which were drawn for both crystal and cluster models. For C−I···Cl−Pt interactions on ELF projections, the I···Cl bond paths go through the lone-pair orange areas of Cl with high ELF values and blue-ish areas with low ELF values around I corresponding to a σ-hole, which confirms the HaB nature of the discussed non-covalent interaction (Figure 10 and Figures S8.3−S8.12).[72−75] The analysis of the 1D profiles of electron density (ED) and
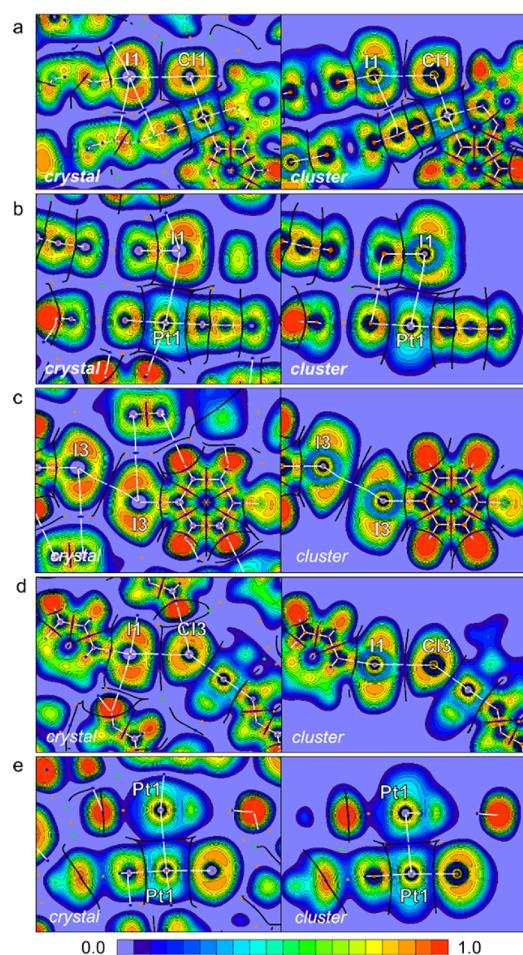
Figure 10. ELF projections (contour lines with a 0.05 step), bond paths (white lines), zero-flux surface projections (black lines), bond CPs (blue dots), nuclear CPs (brown dots), and ring CPs (orange dots) for the I···Cl HaBs in 2^I (a) and 2^{II} (d); Pt···I semicoordination in 2^I (b); and I···I interactions in 2^I (c) and Pt···Pt interactions in 2^{II} (e) in the crystal (left) and cluster (right) models.

electrostatic potential (ESP) functions[76] along the I···Cl bond paths shows a clear shift of the ESP minimum toward the nucleophilic Cl atom, whereas the ED minimum shifts toward the electrophilic I atom in all cases (Figure 11 and Figures S8.3−S8.12). This data confirmed the nucleophilic nature of the chloride ligand and the electrophilic character of I centers of arene isocyanides.

In the structure of 2^I, the Pt···I bond path on the ELF projections passes through the area that corresponds to the region of lone electron pairs of the I atoms and through the area of Pt atoms with a smaller ELF value than that for the I atoms. Analysis of these values verified the nucleophilicity of the I atom toward the Pt center. Thus, the Pt atom functions as an electrophile, while the I center acts as a nucleophile, and consequently, the Pt···I interaction should be treated as the semicoordination.

ELF analysis indicated the nonpolar non-covalent nature of the I···I and Pt···Pt interactions. Further confirmation of the nonpolar nature of the metallophilic interactions is provided by the 1D profiles of the ED and ESP functions along the Pt···Pt bond paths where ED and ESP minima overlap in both cases (Figure 11).

3. CONCLUSIONS

In this study, we prepared four new cyclometalated platinum-(II) complexes (**1−4**) whose solid-state luminescence depend on the aggregation motifs. Complex **2**, which was crystallized in two polymorphic forms 2^I and 2^{II}, shows green and orange phosphorescence, respectively. The other studied solid luminophores, namely, **1**, 3^{I-II}, **4**, and **4·CHCl₃**, exhibit green luminescence. All yellow crystals (**1**, 2^I, 3^I, 3^{II}, **4**, and **4·CHCl₃**) demonstrated a reversible mechanochromic green-to-orange color change achieved by mechanical grinding (green-to-orange) and solvent adsorption (orange-to-green).

The most interesting finding of this work is that orange polymorph 2^{II} exhibits a significantly higher EQY (12%), while 2^I is a very weak emitter (0.5%). One of most significant differences in the structure-determining non-covalent inter-actions between the two polymorphs, that is 2^I and 2^{II}, is seen in the availability of Pt···Pt interactions in 2^{II} and absence of
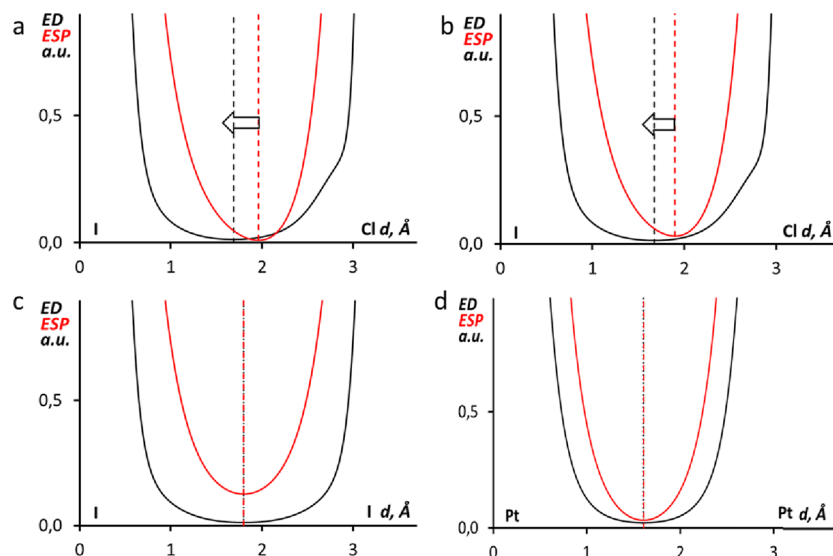

Figure 11. ED (black) vs ESP (red) minima along the bond paths for the I···Cl HaBs in 2^I (a) and 2^{II} (b), I···I interactions in 2^I (c), and Pt···Pt interactions in 2^{II} (d).

these metallophilic contacts in 2^I. Based on our data and previous observations[29,30,42] considered in the Introduction, we hypothesized that the 24-fold difference in the phosphorescence EQYs between polymorphs 2^I and 2^{II} could be related to the presence and absence of Pt···Pt interactions; these metallophilic interactions are accompanied by the reduction of vibrational relaxation due to the formation of a rigid supramolecular structure.

We hope that our results, in conjunction with relevant data of the other studies focused on packing effects in emission performance properties,[36,40] add to the modulation of photophysical properties of organometallic luminescent materials by planned selection of non-covalent interactions.

4. EXPERIMENTAL SECTION

4.1. Materials and Instrumentation. For details, see Section S1. The latter includes the reagents and materials used, photophysical data, X-ray structure determination, and computation details.

4.2. Synthesis of 1−4. $[\{Pt(ppy)(\mu\text{-}Cl)\}_2]$ (50 mg, 0.065 mmol) was suspended in MeCN (2 mL), whereupon a solution of isocyanide (0.130 mmol) in MeCN (2 mL) was added dropwise. The reaction mixture was refluxed at 90 °C for 3 h. During this period, the reaction mixture gradually turned from a yellow suspension to a light yellow solution (for **1−3**) or a yellow suspension (for **4**). After refluxing for 3 h followed by cooling to RT, Et_2O (3 mL) was added to the reaction mixture, and then it was left to stand without stirring for 3 days at RT. In each case, the formed solid was separated by centrifugation, washed with three 3 mL portions of Et_2O, and dried in air at RT. Complexes **1−4** are shelf-stable at RT; they are soluble in aprotic solvents such as CH_2Cl_2 and $CHCl_3$.

4.3. Characterization. Characterization and elemental analyses (C, H, and N), high-resolution ESI⁺-MS, IR, and ^1H, $^{13}C\{^1H\}$, and $^{195}Pt\{^1H\}$ NMR spectroscopy are included in Section S2.

4.4. Crystal Growth. Crystals of **1** were obtained by slow evaporation of its CH_2Cl_2 solution at RT; they were also obtained by slow evaporation of their $CHCl_3$, MeCN, or EtCN solutions at RT. Crystals of 2^I were obtained by slow evaporation of solution of **2** in CH_2Cl_2 at RT. Crystals of 2^{II} were obtained by slow evaporation of solution of **2** in EtCN solutions at RT. Crystals of 3^I were obtained by slow evaporation of solution of **3** in MeCN at 60 °C. Crystals of 3^{II} were obtained by slow evaporation of solution of **2** in $CH_2Cl_2/MeNO_2$ (3:1, v/v) solvent mixture at RT. Crystals of **4** were obtained by slow evaporation of solution of **4** in a CH_2Cl_2/hexane (3:1, v/v) solvent mixture at RT. Crystals of **4·** $CHCl_3$ were obtained by slow evaporation of a solution of **4** in $CHCl_3$ at RT. Slow evaporation of solutions of **3** or **4** in EtCN gives only oily samples, and all our attempts to obtain crystals suitable for XRD studies failed.

ASSOCIATED CONTENT

Supporting Information

The Supporting Information is available free of charge at https://pubs.acs.org/doi/10.1021/acsomega.2c04110.

> Experimental section and spectra, X-ray diffraction, and photophysical data, experimental data and structural-feature discussion, and theoretical calculations (PDF)

AUTHOR INFORMATION

Corresponding Authors

Mikhail A. Kinzhalov − *Saint Petersburg State University, Saint Petersburg 199034, Russian Federation; Research School of Chemistry and Applied Biomedical Sciences, Tomsk Polytechnic University, Tomsk 634050, Russian Federation;* orcid.org/0000-0001-5055-1212; Email: m.kinzhalov@ spbu.ru

Nadezhda A. Bokach − *Saint Petersburg State University, Saint Petersburg 199034, Russian Federation; Research School of Chemistry and Applied Biomedical Sciences, Tomsk Polytechnic University, Tomsk 634050, Russian Federation;* orcid.org/0000-0001-8692-9627; Email: n.bokach@ spbu.ru

Authors

Elina V. Sokolova − *Saint Petersburg State University, Saint Petersburg 199034, Russian Federation;* orcid.org/0000-0001-8857-9536

Andrey S. Smirnov − *Saint Petersburg State University, Saint Petersburg 199034, Russian Federation;* orcid.org/0000-0001-9444-2069

Anna M. Cheranyova − *Saint Petersburg State University, Saint Petersburg 199034, Russian Federation*

Daniil M. Ivanov − *Saint Petersburg State University, Saint Petersburg 199034, Russian Federation; Research School of Chemistry and Applied Biomedical Sciences, Tomsk Polytechnic University, Tomsk 634050, Russian Federation;* orcid.org/0000-0002-0855-2251

Vadim Yu. Kukushkin − *Saint Petersburg State University, Saint Petersburg 199034, Russian Federation; Institute of Chemistry and Pharmaceutical Technologies, Altai State University, Barnaul 656049, Russian Federation;* orcid.org/0000-0002-2253-085X

Complete contact information is available at:
https://pubs.acs.org/10.1021/acsomega.2c04110

Notes

The authors declare no competing financial interest.

REFERENCES

(1) Li, X.; Xie, Y.; Li, Z. Diversity of Luminescent Metal Complexes in OLEDs: Beyond Traditional Precious Metals. *Chem. — Asian J.* **2021**, *16*, 2817−2829.

(2) Mahoro, G. U.; Fernandez-Cestau, J.; Renaud, J.-L.; Coto, P. B.; Costa, R. D.; Gaillard, S. Recent Advances in Solid-State Lighting Devices Using Transition Metal Complexes Exhibiting Thermally Activated Delayed Fluorescent Emission Mechanism. *Adv. Opt. Mater.* **2020**, *8*, 2000260.

(3) Lee, S.; Han, W.-S. Cyclometalated Ir(III) complexes towards blue-emissive dopant for organic light-emitting diodes: fundamentals

of photophysics and designing strategies. *Inorg. Chem. Front.* **2020**, *7*, 2396−2422.

(4) Zhuang, Y.; Guo, S.; Deng, Y.; Liu, S.; Zhao, Q. Electroluminochromic Materials and Devices Based on Metal Complexes. *Chem. − Asian J.* **2019**, *14*, 3791−3802.

(5) Zhang, Q.-C.; Xiao, H.; Zhang, X.; Xu, L.-J.; Chen, Z.-N. Luminescent oligonuclear metal complexes and the use in organic light-emitting diodes. *Chem. Soc. Rev.* **2019**, *378*, 121−133.

(6) Ibrahim-Ouali, M.; Dumur, F. Recent Advances on Metal-Based Near-Infrared and Infrared Emitting OLEDs. *Molecules* **2019**, *24*, 1412.

(7) Tang, M. C.; Chan, A. K. W.; Chan, M. Y.; Yam, V. W. W. Platinum and Gold Complexes for OLEDs. *Top. Curr. Chem.* **2016**, *374*, 46.

(8) Zhou, X.; Lee, S.; Xu, Z.; Yoon, J. Recent Progress on the Development of Chemosensors for Gases. *Chem. Rev.* **2015**, *115*, 7944−8000.

(9) Ma, D.-L.; Wong, S.-Y.; Kang, T.-S.; Ng, H.-P.; Han, Q.-B.; Leung, C.-H. Iridium(III)-based chemosensors for the detection of metal ions. *Methods* **2019**, *168*, 3−17.

(10) Ma, D. L.; Wu, C.; Li, G.; Leung, C. H. Group 8−9 Metal-Based Luminescent Chemosensors for Protein Biomarker Detection. *J. Anal. Test.* **2018**, *2*, 77−89.

(11) Eremina, A. A.; Kinzhalov, M. A.; Katlenok, E. A.; Smirnov, A. S.; Andrusenko, E. V.; Pidko, E. A.; Suslonov, V. V.; Luzyanin, K. V. Phosphorescent Iridium(III) Complexes with Acyclic Diaminocarbene Ligands as Chemosensors for Mercury. *Inorg. Chem.* **2020**, *59*, 2209−2222.

(12) Chan, A. Y.; Perry, I. B.; Bissonnette, N. B.; Buksh, B. F.; Edwards, G. A.; Frye, L. I.; Garry, O. L.; Lavagnino, M. N.; Li, B. X.; Liang, Y.; Mao, E.; Millet, A.; Oakley, J. V.; Reed, N. L.; Sakai, H. A.; Seath, C. P.; MacMillan, D. W. C. Metallaphotoredox: The Merger of Photoredox and Transition Metal Catalysis. *Chem. Rev.* **2021**, 1485.

(13) Glaser, F.; Wenger, O. S. Recent progress in the development of transition-metal based photoredox catalysts. *Coord. Chem. Rev.* **2020**, *405*, No. 213129.

(14) Arias-Rotondo, D. M.; McCusker, J. K. The photophysics of photoredox catalysis: a roadmap for catalyst design. *Chem. Soc. Rev.* **2016**, *45*, 5803−5820.

(15) Prier, C. K.; Rankic, D. A.; MacMillan, D. W. C. Visible Light Photoredox Catalysis with Transition Metal Complexes: Applications in Organic Synthesis. *Chem. Rev.* **2013**, *113*, 5322−5363.

(16) Chi, Y.; Chou, P.-T. Transition-metal phosphors with cyclometalating ligands: fundamentals and applications. *Chem. Soc. Rev.* **2010**, *39*, 638−655.

(17) To, W.-P.; Wan, Q.; Tong, G. S. M.; Che, C.-M. Recent Advances in Metal Triplet Emitters with d(6), d(8), and d(10) Electronic Configurations. *Trends Chem.* **2020**, *2*, 796−812.

(18) Haque, A.; Xu, L.; Al-Balushi, R. A.; Al-Suti, M. K.; Ilmi, R.; Guo, Z.; Khan, M. S.; Wong, W.-Y.; Raithby, P. R. Cyclometallated tridentate platinum(ii) arylacetylide complexes: old wine in new bottles. *Chem. Soc. Rev.* **2019**, *48*, 5547−5563.

(19) Li, K.; Chen, Y.; Wang, J.; Yang, C. Diverse emission properties of transition metal complexes beyond exclusive single phosphorescence and their wide applications. *Coord. Chem. Rev.* **2021**, *433*, No. 213755.

(20) Yam, V. W. W.; Law, A. S. Y. Luminescent d(8) metal complexes of platinum(II) and gold(III): From photophysics to photofunctional materials and probes. *Coord. Chem. Rev.* **2020**, *414*, No. 213298.

(21) Kinzhalov, M. A.; Grachova, E. V.; Luzyanin, K. V. Tuning the Luminescence of Transition Metal Complexes with Acyclic Diaminocarbene Ligands. *Inorg. Chem. Front.* **2022**, *9*, 417−439.

(22) Sutton, G. D.; Olumba, M. E.; Nguyen, Y. H.; Teets, T. S. The diverse functions of isocyanides in phosphorescent metal complexes. *Dalton Trans.* **2021**, *50*, 17851−17863.

(23) Jain, V. K. Cyclometalated group-16 compounds of palladium and platinum: Challenges and opportunities. *Coord. Chem. Rev.* **2021**, *427*, No. 213546.

(24) Cruz-Cabeza, A. J.; Reutzel-Edens, S. M.; Bernstein, J. Facts and fictions about polymorphism. *Chem. Soc. Rev.* **2015**, *44*, 8619−8635.

(25) Lu, B.; Liu, S.; Yan, D. Recent advances in photofunctional polymorphs of molecular materials. *Chin. Chem. Lett.* **2019**, *30*, 1908−1922.

(26) Wang, C.; Li, Z. Molecular conformation and packing: their critical roles in the emission performance of mechanochromic fluorescence materials. *Mater. Chem. Front.* **2017**, *1*, 2174−2194.

(27) Norton, A. E.; Abdolmaleki, M. K.; Liang, J.; Sharma, M.; Golsby, R.; Zoller, A.; Krause, J. A.; Connick, W. B.; Chatterjee, S. Phase transformation induced mechanochromism in a platinum salt: a tale of two polymorphs. *Chem. Commun.* **2020**, *56*, 10175−10178.

(28) Han, Y.; Gao, Z.; Wang, C.; Zhong, R.; Wang, F. Recent progress on supramolecular assembly of organoplatinum(II) complexes into long-range ordered nanostructures. *Coord. Chem. Rev.* **2020**, *414*, No. 213300.

(29) Ohno, K.; Hasebe, M.; Nagasawa, A.; Fujihara, T. Change in Luminescence Induced by Solution-Mediated Phase-Transition of Cyclometalated Platinum(II) Complex with Isoquinoline Carboxylate. *Inorg. Chem.* **2017**, *56*, 12158−12168.

(30) Ikeshita, M.; Ito, M.; Naota, T. Variations in the Solid-State Emissions of Clothespin-Shaped Binuclear trans-Bis-(salicylaldiminato)platinum(II) with Halogen Functionalities. *Eur. J. Inorg. Chem.* **2019**, *2019*, 3561−3571.

(31) Katkova, S. A.; Mikherdov, A. S.; Sokolova, E. V.; Novikov, A. S.; Starova, G. L.; Kinzhalov, M. A. Intermolecular (Isocyano group)···PtII interactions involving coordinated isocyanides in cyclometalated PtII complexes. *J. Mol. Struct.* **2022**, *1253*, No. 132230.

(32) Tiekink, E. R. T. Supramolecular assembly based on "emerging" intermolecular interactions of particular interest to coordination chemists. *Coord. Chem. Rev.* **2017**, *345*, 209−228.

(33) Aliprandi, A.; Genovese, D.; Mauro, M.; Cola, L. D. Recent Advances in Phosphorescent Pt(II) Complexes Featuring Metallophilic Interactions: Properties and Applications. *Chem. Lett.* **2015**, *44*, 1152−1169.

(34) Gray, H. B.; Záliš, S.; Vlček, A. Electronic structures and photophysics of d8-d8 complexes. *Coord. Chem. Rev.* **2017**, *345*, 297−317.

(35) Yoshida, M.; Kato, M. Regulation of metal−metal interactions and chromic phenomena of multi-decker platinum complexes having π-systems. *Coord. Chem. Rev.* **2018**, *355*, 101−115.

(36) Ravotto, L.; Ceroni, P. Aggregation induced phosphorescence of metal complexes: From principles to applications. *Coord. Chem. Rev.* **2017**, *346*, 62−76.

(37) Sivchik, V. V.; Solomatina, A. I.; Chen, Y. T.; Karttunen, A. J.; Tunik, S. P.; Chou, P. T.; Koshevoy, I. O. Halogen Bonding to Amplify Luminescence: A Case Study Using a Platinum Cyclometalated Complex. *Angew. Chem., Int. Ed.* **2015**, *54*, 14057−14060.

(38) Sivchik, V.; Sarker, R. K.; Liu, Z.-Y.; Chung, K.-Y.; Grachova, E. V.; Karttunen, A. J.; Chou, P.-T.; Koshevoy, I. O. Improvement of the Photophysical Performance of Platinum-Cyclometalated Complexes in Halogen-Bonded Adducts. *Chem. − Eur. J.* **2018**, *24*, 11475−11484.

(39) Katkova, S. A.; Luzyanin, K. V.; Novikov, A. S.; Kinzhalov, M. A. Modulation of luminescence properties for [cyclometalated]-PtII(isocyanide) complexes upon co-crystallisation with halosubstituted perfluorinated arenes. *New J. Chem.* **2021**, *45*, 2948−2952.

(40) Koshevoy, I. O.; Krause, M.; Klein, A. Non-covalent intramolecular interactions through ligand-design promoting efficient photoluminescence from transition metal complexes. *Coord. Chem. Rev.* **2020**, *405*, No. 213094.

(41) Unesaki, H.; Kato, T.; Watase, S.; Matsukawa, K.; Naka, K. Polymorph Control of Luminescence Properties in Molecular Crystals of a Platinum and Organoarsenic Complex and Formation of Stable One-Dimensional Nanochannel. *Inorg. Chem.* **2014**, *53*, 8270−8277.

(42) Pinter, P.; Hennersdorf, F.; Weigand, J. J.; Strassner, T. Polymorphic Phosphorescence from Separable Aggregates with Unique Photophysical Properties. *Chem. Eur. J.* **2021**, *27*, 13135.

(43) Kuwabara, J.; Yamaguchi, K.; Yamawaki, K.; Yasuda, T.; Nishimura, Y.; Kanbara, T. Modulation of the Emission Mode of a Pt(II) Complex via Intermolecular Interactions. *Inorg. Chem.* **2017**, *56*, 8726−8729.

(44) Fuertes, S.; Chueca, A. J.; Peralvarez, M.; Borja, P.; Torrell, M.; Carreras, J.; Sicilia, V. White Light Emission from Planar Remote Phosphor Based on NHC Cycloplatinated Complexes. *ACS Appl. Mater. Interfaces* **2016**, *8*, 16160−16169.

(45) Dobrynin, M. V.; Sokolova, E. V.; Kinzhalov, M. A.; Smirnov, A. S.; Starova, G. L.; Kukushkin, V. Y.; Islamova, R. M. Cyclometalated Platinum(II) Complexes Simultaneously Catalyze the Cross-Linking of Polysiloxanes and Function as Luminophores. *ACS Appl. Polym. Mater.* **2021**, *3*, 857−866.

(46) Martínez-Junquera, M.; Lara, R.; Lalinde, E.; Moreno, M. T. Isomerism, aggregation-induced emission and mechanochromism of isocyanide cycloplatinated(ii) complexes. *J. Mater. Chem. C* **2020**, *8*, 7221−7233.

(47) Spackman, M. A.; Jayatilaka, D. Hirshfeld surface analysis. *CrystEngComm* **2009**, *11*, 19−32.

(48) Bondi, A. Van der Waals Volumes and Radii. *J. Phys. Chem.* **1964**, *68*, 441−451.

(49) Alvarez, S. A cartography of the van der Waals territories. *Dalton Trans.* **2013**, *42*, 8617−8636.

(50) Pedireddi, V. R.; Reddy, D. S.; Goud, B. S.; Craig, D. C.; Rae, A. D.; Desiraju, G. R. The nature of halogen ··· halogen interactions and the crystal structure of 1,3,5,7-tetraiodoadamantane. *J. Chem.Soc., Perkin Trans.* **1994**, *11*, 2353−2360.

(51) Mukherjee, A.; Desiraju, G. R. Halogen bonds in some dihalogenated phenols: applications to crystal engineering. *IUCrJ* **2014**, *1*, 49−60.

(52) Xue, P.; Ding, J.; Wang, P.; Lu, R. Recent progress in the mechanochromism of phosphorescent organic molecules and metal complexes. *J. Mater. Chem. C* **2016**, *4*, 6688−6706.

(53) Soto, M. A.; Kandel, R.; MacLachlan, M. J. Chromic Platinum Complexes Containing Multidentate Ligands. *Eur. J. Inorg. Chem.* **2021**, *2021*, 894−906.

(54) Han, A.; Du, P.; Sun, Z.; Wu, H.; Jia, H.; Zhang, R.; Liang, Z.; Cao, R.; Eisenberg, R. Reversible Mechanochromic Luminescence at Room Temperature in Cationic Platinum(II) Terpyridyl Complexes. *Inorg. Chem.* **2014**, *53*, 3338−3344.

(55) Li, J.; Chen, K.; Wei, J.; Ma, Y.; Zhou, R.; Liu, S.; Zhao, Q.; Wong, W.-Y. Reversible On−Off Switching of Excitation-Wavelength-Dependent Emission of a Phosphorescent Soft Salt Based on Platinum(II) Complexes. *J. Am. Chem. Soc.* **2021**, *143*, 18317−18324.

(56) Zhang, X.-P.; Mei, J.-F.; Lai, J.-C.; Li, C.-H.; You, X.-Z. Mechano-induced luminescent and chiroptical switching in chiral cyclometalated platinum(II) complexes. *J. Mater. Chem. C* **2015**, *3*, 2350−2357.

(57) Krikorian, M.; Liu, S.; Swager, T. M. Columnar Liquid Crystallinity and Mechanochromism in Cationic Platinum(II) Complexes. *J. Am. Chem. Soc.* **2014**, *136*, 2952−2955.

(58) Ohno, K.; Yamaguchi, S.; Nagasawa, A.; Fujihara, T. Mechanochromism in the luminescence of novel cyclometalated platinum(II) complexes with alpha-aminocarboxylates. *Dalton Trans.* **2016**, *45*, 5492−5503.

(59) Lin, C.-J.; Liu, Y.-H.; Peng, S.-M.; Shinmyozu, T.; Yang, J.-S. Excimer−Monomer Photoluminescence Mechanochromism and Vapochromism of Pentiptycene-Containing Cyclometalated Platinum(II) Complexes. *Inorg. Chem.* **2017**, *56*, 4978−4989.

(60) Puttock, E. V.; Walden, M. T.; Williams, J. A. G. The luminescence properties of multinuclear platinum complexes. *Coord. Chem. Rev.* **2018**, *367*, 127−162.

(61) Politzer, P.; Lane, P.; Concha, M. C.; Ma, Y.; Murray, J. S. An overview of halogen bonding. *J. Mol. Model.* **2007**, *13*, 305−311.

(62) Politzer, P.; Murray, J. S.; Clark, T. Halogen bonding: an electrostatically-driven highly directional noncovalent interaction. *Phys. Chem. Chem. Phys.* **2010**, *12*, 7748−7757.

(63) Cox, S. R.; Williams, D. E. Representation of the molecular electrostatic potential by a net atomic charge model. *J. Comput. Chem.* **1981**, *2*, 304−323.

(64) Contreras-García, J.; Johnson, E. R.; Keinan, S.; Chaudret, R.; Piquemal, J.-P.; Beratan, D. N.; Yang, W. NCIPLOT: A Program for Plotting Noncovalent Interaction Regions. *J. Chem. Theory Comput.* **2011**, *7*, 625−632.

(65) Lefebvre, C.; Rubez, G.; Khartabil, H.; Boisson, J.-C.; Contreras-García, J.; Hénon, E. Accurately extracting the signature of intermolecular interactions present in the NCI plot of the reduced density gradient versus electron density. *Phys. Chem. Chem. Phys.* **2017**, *19*, 17928−17936.

(66) Becke, A. D.; Edgecombe, K. E. A simple measure of electron localization in atomic and molecular systems. *J. Phys. Chem.* **1990**, *92*, 5397−5403.

(67) Silvi, B.; Savin, A. Classification of chemical bonds based on topological analysis of electron localization functions. *Nature* **1994**, *371*, 683−686.

(68) Savin, A.; Nesper, R.; Wengert, S.; Fässler, T. F. ELF: The Electron Localization Function. *Angew. Chem., Int. Ed.* **1997**, *36*, 1808−1832.

(69) Bader, R. F. W. A quantum theory of molecular structure and its applications. *Chem. Rev.* **1991**, *91*, 893−928.

(70) Clark, T.; Hennemann, M.; Murray, J. S.; Politzer, P. Halogen bonding: the σ-hole. *J. Mol. Model.* **2007**, *13*, 291−296.

(71) Politzer, P.; Murray, J. S.; Clark, T. Halogen bonding and other [sigma]-hole interactions: a perspective. *Phys. Chem. Chem. Phys.* **2013**, *15*, 11178−11189.

(72) Bartashevich, E.; Yushina, I.; Kropotina, K.; Muhitdinova, S.; Tsirelson, V. Testing the tools for revealing and characterizing the iodine-iodine halogen bond in crystals. *Acta Crystallogr. B* **2017**, *73*, 217−226.

(73) Masaryk, L.; Moncol, J.; Herchel, R.; Nemec, I. Halogen Bonding in New Dichloride-Cobalt(II) Complex with Iodo Substituted Chalcone Ligands. *Crystals* **2020**, *10*, 354.

(74) Bulatova, M.; Ivanov, D. M.; Haukka, M. Classics Meet Classics: Theoretical and Experimental Studies of Halogen Bonding in Adducts of Platinum(II) 1,5-Cyclooctadiene Halide Complexes with Diiodine, Iodoform, and 1,4-Diiodotetrafluorobenzene. *Cryst. Growth Des.* **2021**, *21*, 974−987.

(75) Eliseeva, A. A.; Ivanov, D. M.; Rozhkov, A. V.; Ananyev, I. V.; Frontera, A.; Kukushkin, V. Y. Bifurcated Halogen Bonding Involving Two Rhodium(I) Centers as an Integrated σ-Hole Acceptor. *JACS Au* **2021**, *1*, 354−361.

(76) Zhao, N.; Wu, Y.-H.; Luo, J.; Shi, L.-X.; Chen, Z.-N. Aggregation-induced phosphorescence of iridium(iii) complexes with 2,2′-bipyridine-acylhydrazone and their highly selective recognition to Cu2+. *Analyst* **2013**, *138*, 894−900.